

Digital Complex Signal Processing Techniques for Impulse Radio

Mike Shuo-Wei Chen, and Robert W. Brodersen

Abstract—This paper describes the digital complex signal processing techniques for a pulse-based UWB radio. The proposed baseband is essential to fully exploit the wideband signal characteristics as well as compensating the analog front-end impairments. The property and optimal usage of these signal processing blocks are analyzed for both data detection and precision ranging applications. The same signal processing approaches are applicable for baseband and passband UWB communications as both are of interest under FCC regulations.

I. INTRODUCTION

Ultra-wideband (UWB) transmission was approved by the FCC in 2002 [1] for several frequency bands (0-960 MHz, 3.1-10.6 GHz and 22-29 GHz), and has since drawn considerable attention for a variety of applications, including imaging, surveillance, high-speed data communication and high-resolution locationing [2][3]. Among these, an indoor communication system operated in the frequency band from 3.1 to 10.6 GHz is targeted for high-speed (100s' of Mb/s) and short-range (less than 10 meters) systems, such as wireless personal area network (WPAN). On the other extreme, low data rate (10s' Kb/s) but ultra low power communications are of interest, such as sensor network. Due to the wide usable bandwidth, UWB also owns a great potential for precision ranging/positioning systems.

Among the several possible signalling techniques, we have explored the non-sinusoidal carrier approach, so called impulse radios [4][5], which allowed us to take a fundamentally new approach to radio architectures [6], signal processing techniques, and analog circuits. In this paper, we focus on exploiting digital signal processing techniques to take the benefit of the wideband characteristics of UWB pulses and seek to dramatically cut down the implementation cost and explore the inherent fine-timing resolution simultaneously.

The paper is organized as follows. Section II compares different complex signal representations of UWB signals and examples of these transformations will be shown using FIR implementations. Section III proposes a digital backend based on the described complex signal transformations. The performance of the critical signal processing blocks is analyzed. The proper usage for data detection and ranging is also discussed.

II. COMPLEX REPRESENTATIONS OF UWB SIGNALS

To understand the time information extraction, a sampling offset is purposely injected in the time domain and the change in the frequency domain is observed. Equation (1) shows a bandlimited signal, $s(t)$, sampled at sampling rate, $1/T_s$. Whenever there is a sampling offset, T_o , it will cause a phase shift, $e^{-jk\frac{2\pi}{T_s}T_o}$, in the frequency domain.

$$s(t) \cdot \sum \delta(t-k \cdot T_s - T_o) \xLeftrightarrow{\mathcal{F}, \mathcal{T}} S(\omega) * \sum \delta(\omega - k \frac{2\pi}{T_s}) \cdot e^{-jk \frac{2\pi}{T_s} T_o}. \quad (1)$$

The key to study phase information is to project the signal into an orthogonal space, i.e. a 90-degree phase shift in this case. In a narrowband system, sine and cosine are orthogonal to each other, and often referred as I and Q channel. However, for an UWB signal, the orthogonality at one particular frequency is not sufficient, and thus a wideband phase shifter is in need. Concerning the reasonable implementation cost, two operators are compared: Hilbert transformer ($\mathcal{H}[\cdot]$) and the differentiator ($\mathcal{D}[\cdot]$). A wideband 90-degree phase shift is obtained, as seen in their ideal frequency response, Eq. (2) and (3).

$$\mathcal{H}[s(t)] = \frac{1}{\pi t} * s(t) \xLeftrightarrow{\mathcal{F}, \mathcal{T}} -j \cdot \text{sign}(\omega) \cdot S(\omega) \quad (2)$$

where $\text{sign}()$ is the signum function.

$$\mathcal{D}[s(t)] = \frac{d}{dt} \cdot s(t) \xLeftrightarrow{\mathcal{F}, \mathcal{T}} j \cdot \omega \cdot S(\omega) \quad (3)$$

Note that, in both cases, 90-degree phase shift is independent of the frequency. For a narrowband signal, i.e. $\sin(\omega_o t)$, the two operators are almost identical except a constant gain difference, because $\mathcal{H}(\sin(\omega_o t)) = \cos(\omega_o t)$ while $\mathcal{D}(\sin(\omega_o t)) = \omega_o \cdot \cos(\omega_o t)$. However, in a wideband signal case, the differentiator suffers from a non-flat gain response (proportional to frequency) as seen in Eq. (3), which will not only introduce signal distortion, but also enhance the unwanted noise at high frequency. In contrast, an ideal Hilbert transformer has unity gain over the entire spectrum, which avoids any signal distortion.

To implement these operations in digital baseband, the discrete Hilbert transformer and differentiator are examined. As an example, we design an equal-ripple 21-tap FIR filter using Parks-McClellan algorithm to obtain exact 90-degree phase shift for Hilbert transformer [7]. For the differentiator, a backward difference approximation ($y[n] = x[n] - x[n-1]$) and central difference approximation ($y[n] = (x[n+1] - x[n-1])/2$) are considered for their simplicity in computation. We also design a 21-tap FIR filter for differentiator using Parks-McClellan algorithm. The phase response of these discrete-time implementations all remains 90 degree. However, in terms of magnitude response, the discrete Hilbert transformer has the widest bandwidth and least passband ripple, and therefore

serves as the optimal operator in minimizing distortion for such a wideband system.

With the assistance of phase shifters, we can combine these orthogonal bases into a complex signal. By combining Hilbert transformed signal, a single-side banded (SSB) spectrum, so called analytic signal, is derived as $y(t) = s(t) + j \cdot \mathcal{H}(s(t))$. Similarly, for a narrowband signal centered at ω_o , a complex signal, which is an approximation of analytic signal, can be formulated as $y(t) = s(t) + j \cdot \frac{1}{\omega_o} \mathcal{D}(s(t))$.

To better understand what these complex signal represents for UWB pulses, these transformations are applied for both baseband and passband wideband signal, since FCC allows both below 1 GHz and 3-10 GHz frequency bands. Figure 1 shows the real and imaginary part of the transformed complex signal and its magnitude and phase information. Due to the large passband ripple in the frequency response, using differentiator approach causes more pulse distortion. Therefore, its complex representation less reflects the true shape of the UWB pulse.

III. PROPOSED DIGITAL BASEBAND USING COMPLEX SIGNALING

Based on complex signalling, Fig. 2 shows the datapath of the proposed digital baseband. The main components are analytic signal transformer, pulse shape estimator, correlators, analytic matched filter, and detection block. For optimal detection, the sufficient statistics is achieved by projecting onto the signal dimension through pulse matched filtering whose filter response requires an estimation block. The following correlators are used to provide more processing gain if necessary or despread any possible modulated code. Finally, a detection block makes use of the analytic matched filter outputs to decode the data or extract timing information for ranging purpose. Several critical processing blocks will be discussed in this section.

A. Analytic signal transformer

The analytic signal transformation can be implemented using FIR Hilbert transformer or FFT processor. With FFT approach, one can potentially eliminate in-band tones before the detection block with the penalty of more implementation complexity. From the system simulations, using 21-tap FIR Hilbert transformer degrades SNR by less than 1 dB compared to ideal analytic signal transformation.

B. Pulse shape estimator

To make optimal detection, the pulse matched filter response is required as a priori information. However, due to the varying wireless channel response and antenna pattern, the received pulse shape needs estimation on the receiver side before decoding data [8]. In the proposed baseband, a maximum likelihood (ML) estimator is used as the shape estimation without any prior information. It is assumed that a training sequence spreaded with a pseudo random (PN) code is transmitted within the coherence time of the channel.

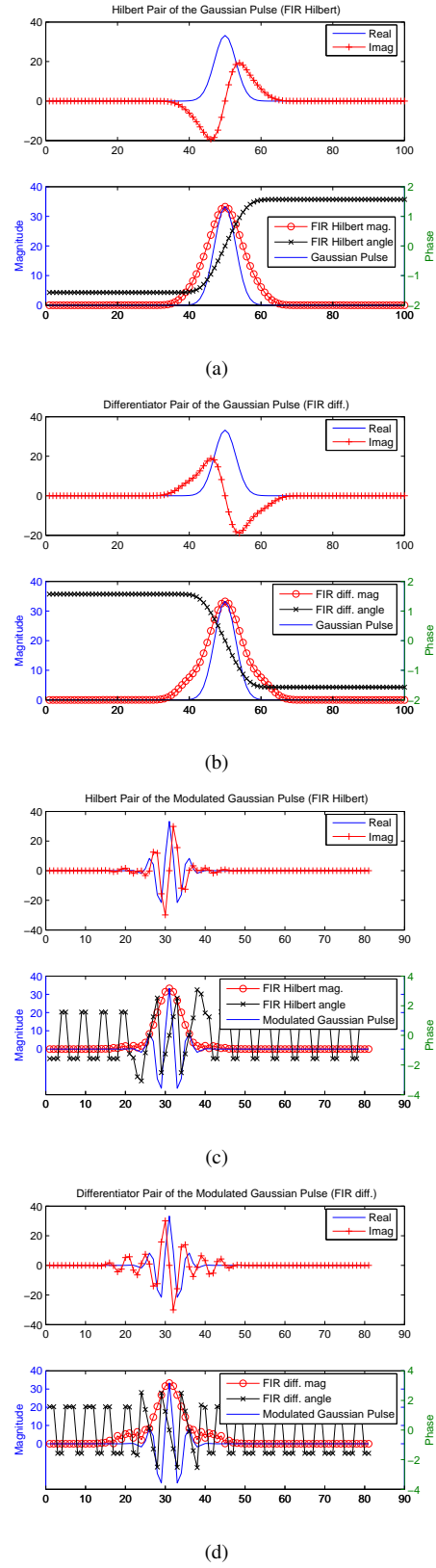


Fig. 1. 21-tap FIR of Hilbert and differentiator operator on Gaussian and modulated Gaussian pulses (a) Hilbert on Gaussian pulse (b) Differentiator on Gaussian pulse (c) Hilbert of modulated Gaussian pulse (d) Differentiator on modulated Gaussian pulse

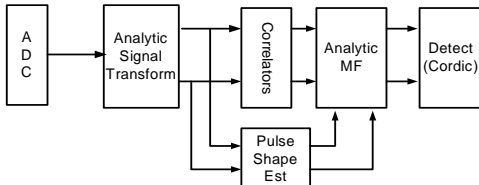
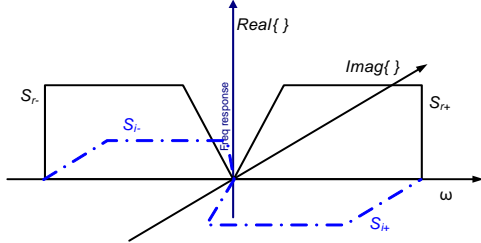
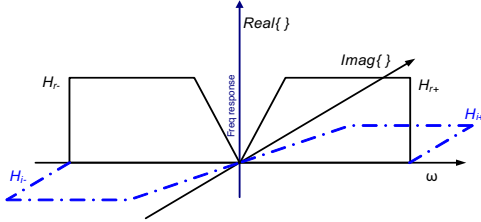


Fig. 2. Datapath of the proposed digital baseband



(a) Signal frequency response, S_r and S_i



(b) Matched filter frequency response, H_r and H_i

Fig. 3. Analytic signal pair of signal and matched filter response

The modulated pulses are spaced far enough to avoid inter-symbol interference during training phase. The ML estimator is essentially running average given a white Gaussian noise.

C. Analytic matched filter

An analytic matched filter is used to achieve optimal performance assuming the incoming noise is additive and white. The assumption is valid if the circuit and ambient thermal noise dominate. For interference dominated case, a whitening filter, which can be incorporated with analytic signal transformer as mentioned earlier, is required for optimal performance. To gain more insights about the analytic matched filter, the expressions of its outputs are derived in continuous time for both noiseless and noisy cases, which can be easily extended for discrete-time case. Assuming the UWB signal, $s(t)$, is transformed into the analytic signal representation, $\tilde{s}(t) = s_r(t) + j \cdot s_i(t)$, the matched filter response is implemented as $\tilde{h}(t) = \tilde{s}^*(T-t) = s_r^*(T-t) - j \cdot s_i^*(T-t)$. We define the impulse response of the filter as $\tilde{h}(t) = h_r(t) - j \cdot h_i(t)$, and thus $h_r(t) = s_r^*(T-t)$, and $h_i(t) = s_i^*(T-t)$. As a result, their Fourier transformed counterparts satisfy $H_r(\omega) = S_r^*(\omega)$ and $H_i(\omega) = S_i^*(\omega)$, as shown in Fig. 3. Note that $s_r(t), s_i(t), h_r(t), h_i(t)$ are real-valued functions.

Before we proceed with further analysis, an operator is defined as follows,

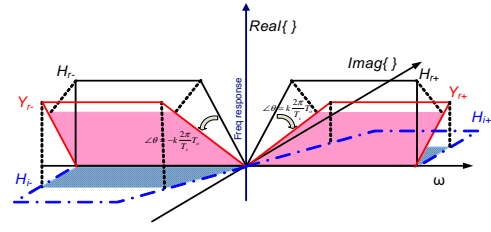


Fig. 4. Graphic view of matched filtering ($\langle Y_r, H_r \rangle$ and $\langle Y_r, H_i \rangle$)

$$\langle x, y \rangle = \int_a^b x(t) \cdot y(T-t) dt, \text{ where } T = b - a. \quad (4)$$

If the inputs of the analytic matched filter are $y_r(t) + j \cdot y_i(t)$, its outputs are expressed as,

$$\begin{aligned} m_r + j \cdot m_i &= \langle y_r + j \cdot y_i, h_r - j \cdot h_i \rangle \\ &= \langle y_r, h_r \rangle + \langle y_i, h_i \rangle \\ &\quad + j \cdot (-\langle y_r, h_i \rangle + \langle y_i, h_r \rangle). \end{aligned} \quad (5)$$

The UWB pulse is assumed to locate between time a and b without inter-symbol interference.

To understand the properties of the analytic matched filter, three conditions are considered for Eq. (5). We begin with an ideal communication channel and gradually add in more non-idealities as shown in the following.

1) *Noiseless input and perfectly matched timing*: This is the ideal case in which incoming signal perfectly matches with the matched filter response without any noise, i.e. $y_r = s_r, y_i = s_i$. The sampling timing offset between input signal and impulse response is assumed zero. The output is expressed as,

$$\begin{aligned} m_r + j \cdot m_i &= \langle s_r + j \cdot s_i, h_r - j \cdot h_i \rangle \\ &= \langle s_r, h_r \rangle + \langle s_i, h_i \rangle \\ &\quad + j \cdot (-\langle s_r, h_i \rangle + \langle s_i, h_r \rangle) \\ &= E_r + E_i = 2 \cdot E_s \end{aligned} \quad (6)$$

, where E_r, E_i is the real and imaginary part of signal energy defined as $\int_a^b s_r^2(t) dt$ and $\int_a^b s_i^2(t) dt$ respectively. We assume an ideal analytic transformer, and thus $E_r = E_i = E_s$. Note that $s_r(t)$ and $h_i(t)$ are orthogonal to each other, therefore $\langle s_r, h_i \rangle = \langle s_i, h_r \rangle = 0$. This shows all the energy concentrates in the real part of the analytic matched filter, and thus complex signal transformation is redundant under the ideal case.

2) *Noiseless input with timing offset*: In this case, a timing offset of T_o is added between input signal and matched filter response while the input is still noiseless. Recall from Eq. (1), the timing offset introduces a phase shift term of $e^{\pm j k \frac{2\pi}{T_s} T_o}$. The frequency response of the real part of the received signal is shown in Fig. 4; $Y_{r\pm}(\omega)$ is rotated by $\pm k \frac{2\pi}{T_s} T_o$ from $H_{r\pm}(\omega)$. Since matched filtering is equivalent to image projection in the

frequency domain, the projected area represents the absolute value of the matched filter output. In Fig. 4, the values of $\langle y_r, h_r \rangle, \langle y_r, h_i \rangle$ are shown in the darker and lighter shaded area. Observing from the graph, the timing offset results in a re-distribution of the signal energy between these two terms. Therefore, complex signal transformation is necessary in this case, otherwise the signal energy will be lost under any timing uncertainty. The matched filter output is re-derived as,

$$\begin{aligned} m_r + j \cdot m_i &= \langle y_r, h_r \rangle + \langle y_i, h_i \rangle \\ &+ j \cdot (\langle y_r, h_i \rangle + \langle y_i, h_r \rangle) \\ &= 2E_s \cdot \cos\theta + j \cdot (-2E_s \cdot \sin\theta) \\ &, \quad \text{where } \theta = k \frac{2\pi}{T_s} T_o. \end{aligned} \quad (7)$$

This equation implies that taking the magnitude of the analytic matched filter output conserves the entire signal energy.

$$\sqrt{m_r^2 + m_i^2} = \sqrt{4E_s^2(\cos^2\theta + \sin^2\theta)} = 2E_s \quad (8)$$

3) *Noisy input with timing offset*: A noise term is added to the inputs to study the filter performance under various signal-to-noise ratio (SNR) and timing offset. The noise is modelled as white Gaussian distribution for the following analysis.

$$\begin{aligned} m_r + j \cdot m_i &= \langle y_r + n_r + j \cdot (y_i + n_i), h_r - j \cdot h_i \rangle \\ &= 2E_s \cdot \cos\theta + n_{mr} \\ &- j \cdot (2E_s \cdot \sin\theta + n_{mi}) \end{aligned} \quad (9)$$

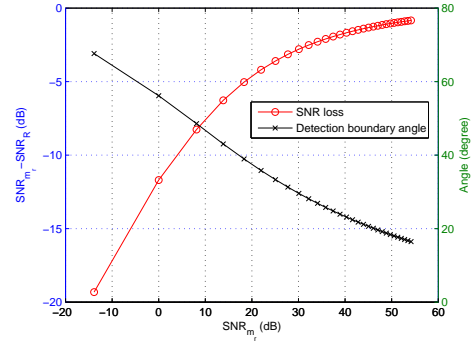
, where the following assumptions are made,

- 1) n_r and n_i are i.i.d.
- 2) $n_{mr} = \langle n_r, h_r \rangle + \langle n_i, h_i \rangle \sim N(0, \sigma_n^2)$
- 3) $n_{mi} = -\langle n_r, h_i \rangle + \langle n_i, h_r \rangle \sim N(0, \sigma_n^2)$

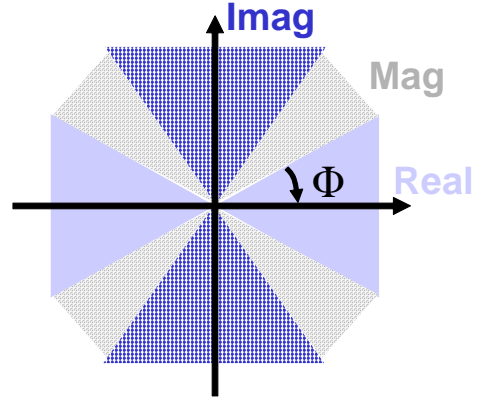
In the case of noiseless input, the magnitude of the analytic matched filter output conserves all the signal energy. However, under the noisy input case, this does not always result in the best performance. For example, when the timing perfectly matches, i.e. all the signal energy resides in the real part, the imaginary part has nothing but noise. Therefore, any operation involving imaginary part has to degrade the overall performance. In the following analysis, we derive the SNR of the magnitude of the matched filter output to compare against that of the real part. The optimal detection region for various input SNR will then be explored.

Given the white Gaussian input noise, the magnitude of the matched filter, $R = \sqrt{m_r^2 + m_i^2}$ is Ricean distribution [9]. To calculate the SNR of R , the Euclidean distance between signal existence and absence is used as signal energy.

$$SNR_R\left(\frac{2E_s}{\sigma_n} = \alpha\right) = \frac{\left(\frac{E(R)|_{\frac{2E_s}{\sigma_n}=\alpha} - E(R)|_{\frac{2E_s}{\sigma_n}=0}}{2}\right)^2}{Var(R)|_{\frac{2E_s}{\sigma_n}=\alpha}}. \quad (10)$$



(a) SNR_{loss} and detection boundary angle (Φ) v.s. input SNR



(b) Optimal detection region

Fig. 5. Detection performance for analytic matched filter

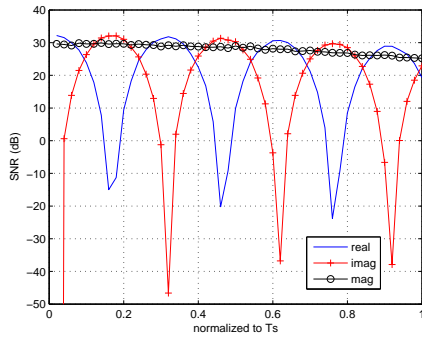
Similarly, the SNR of the real part of the matched filter can be derived as,

$$\begin{aligned} SNR_{m_r}\left(\frac{2E_s}{\sigma_n} = \alpha\right) &= \frac{\left(\frac{E(m_r)|_{\frac{2E_s}{\sigma_n}=\alpha} - E(m_r)|_{\frac{2E_s}{\sigma_n}=0}}{2}\right)^2}{Var(m_r)|_{\frac{2E_s}{\sigma_n}=\alpha}} \\ &= \frac{\alpha^2}{4} \cdot \cos^2\theta. \end{aligned} \quad (11)$$

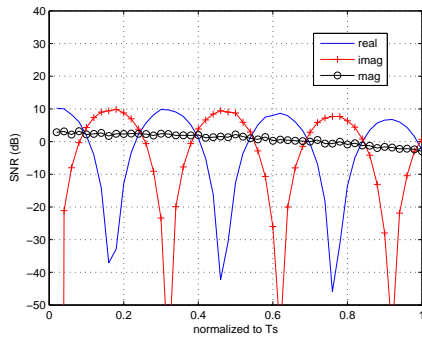
Figure 5(a) shows $SNR_{loss} = SNR_{m_r} - SNR_R$ (in dB) under different input noise level without timing offset, i.e. $\theta = 0$. For the higher SNR regime, SNR degradation is less significant than the lower SNR regime. Due to SNR_{loss} , there exists the optimal detection region where any of the real, imaginary, magnitude part of the matched filter output results in a better performance, as shown in Figure 5(b). The boundary of these detection region can be defined through a detection boundary angle, Φ , which is calculated as,

$$\begin{aligned} SNR_R(\alpha) &\leq SNR_{m_r}(\alpha, \theta) \\ \implies \theta &\leq \Phi = \arccos\left(\sqrt{\frac{4}{\alpha^2} \cdot SNR_R}\right). \end{aligned} \quad (12)$$

Eq. (12) defines the region where the real part of matched filter output performs better. Consequently, if $\Phi > 45$ degree,



(a) Higher SNR



(b) Lower SNR

Fig. 6. SNR of real, imaginary, magnitude part of matched filter output with 0 to $1 T_s$ timing offset with high and low SNR .

the magnitude of the matched filter always performs worse than the real or imaginary part, and should not be used for detection. Note that Φ decreases as SNR increases. In the extremely high SNR case, the magnitude of the matched filter performs the best regardless of the timing offset.

Figure 6 shows SNR of the real, imaginary and magnitude of the matched filter with $[0..T_s]$ timing offset under different input noise level. The Monte-Carlo simulation results confirm that partitioning into three detection regions is necessary for optimal performance in the higher SNR regime, while two is adequate in the lower one.

D. Timing extraction from the proposed baseband

The timing offset can be caused either by circuit impairments or signal arrival time due to the movement between transmitter and receiver or environment changes if it is a non-line-of-sight (NLOS) link. Therefore, the timing information is useful for ranging or tracking application. The complex output of the analytic matched filter essentially provides a 2-D correlation profile of a UWB pulse. As the delay increases from time t_{ref} to $t_{ref} + \Delta t$, the analytic matched filter output moves along a certain trajectory on the Euler plane, as shown in Fig. 7. The movement of the trajectory can be decomposed into two steps. First of all, the matched filter output will trace a baseband signal correlation profile, shown as a heart shape. In the case of a passband pulse, it will further move along a

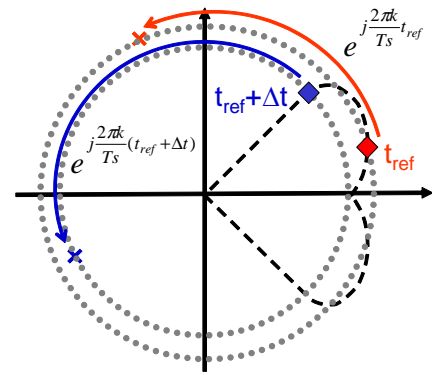


Fig. 7. Trajectory of analytic matched filter output as delay varies

circle with a certain angle depends on the passband frequency (k/T_s) and time delay (Δt). Since each UWB pulse shape has its unique trajectory, it enables the capability of tracking environment changes as the pulse shape can be varied [8]. However, it requires a perfect gain control and a high SNR to precisely locate the position of the trajectory, which will inevitably increase the implementation complexity.

IV. CONCLUSION

A digital backend based on complex signal representation is proposed for baseband and passband UWB communications. By exploiting the analytic matched filter outputs, optimal detection region can be used for synchronization and data communication purpose. On the other hand, the derived 2-D correlation profile allows a fine time resolution, which implies a high accuracy ranging capability.

ACKNOWLEDGMENT

The project was supported by Army Research Office, North Carolina (Award No. 065861) and industrial members of the Berkeley Wireless Research Center.

REFERENCES

- [1] "Revision of part 15 of the commission's rule regarding ultra-wideband transmission systems," *Federal Communications Commission*, First Report and Order, Feb. 2002.
- [2] S. Roy, J. R. Foerster, V. S. Somayazulu, and D. G. Leeper, "Ultrawideband radio design: The promise of high-speed, short-range wireless connectivity," *Proceedings of the IEEE*, vol. 4 Issue 2, pp. 295–311, Feb. 2004.
- [3] G. R. Aiello and G. D. Rogerson, "Ultra-wideband wireless systems," *IEEE Microwave Magazine*, vol. 4 Issue 2, pp. 36–47, June 2003.
- [4] R. A. Scholtz, "Multiple access with time-hopping impulse modulation," *Proc. MILCOM*, vol. 2, pp. 447–450, Oct. 1993.
- [5] I. O'Donnell, M. Chen, S. Wang, and R. Brodersen, "An integrated, low power, ultra-wideband transceiver architecture for low-rate, indoor wireless systems," *IEEE CAS Workshop on Wireless Communications and Networking*, Sept. 2002.
- [6] M. S. W. Chen and R. W. Brodersen, "A subsampling UWB radio architecture by analytic signalling," *Proc. ICASSP*, vol. 4, pp. 533–536, May 2004.
- [7] A. Oppenheim and R. Schaffer, *Discrete-Time Signal Processing 2nd Ed.* Englewood Cliffs, NJ: Prentice Hall, 1998.
- [8] M. S. W. Chen and R. W. Brodersen, "The impact of a wideband channel on UWB system design," *Proc. MILCOM*, vol. 1, pp. 163–168, Nov. 2004.
- [9] J. G. Proakis, *Digital Communications*. New York: McGraw Hill, 1995.